

***In-situ* strain-tuning of the metal-insulator-transition of Ca_2RuO_4
in angle-resolved photoemission experiments**

S. Riccò,¹ M. Kim,^{2,3} A. Tamai,¹ S. McKeown Walker,¹ F. Y. Bruno,¹ I. Cucchi,¹ E. Cappelli,¹ C. Besnard,¹ T. K. Kim,⁴ P. Dudin,⁴ M. Hoesch,^{4,*} M. J. Gutmann,⁵ A. Georges,^{2,3,1,6} R. S. Perry,⁷ and F. Baumberger^{1,8}

¹*Department of Quantum Matter Physics, University of Geneva,
24 Quai Ernest-Ansermet, 1211 Geneva 4, Switzerland*

²*Centre de Physique Théorique Ecole Polytechnique,
CNRS, Université Paris-Saclay, 91128 Palaiseau, France*

³*College de France, 11 place Marcelin Berthelot, 75005 Paris, France*

⁴*Diamond Light Source, Harwell Campus, Didcot, United Kingdom*

⁵*ISIS Neutron and Muon Source, Science and Technology Facilities Council,
Rutherford Appleton Laboratory, Didcot OX11 0QX, United Kingdom*

⁶*Center for Computational Quantum Physics,
Flatiron Institute, 162 5th Avenue, New York, NY 10010, USA*

⁷*London Centre for Nanotechnology and UCL Centre for Materials Discovery,
University College London, London WC1E 6BT, United Kingdom*

⁸*Swiss Light Source, Paul Scherrer Institut, CH-5232 Villigen PSI, Switzerland*

Abstract: We report the evolution of the k -space electronic structure of lightly doped bulk Ca_2RuO_4 with uniaxial strain. Using ultrathin plate-like crystals, we achieve strain levels up to -4.1% , sufficient to suppress the Mott phase and access the previously unexplored metallic state at low temperature. Angle-resolved photoemission experiments performed while tuning the uniaxial strain reveal that metallicity emerges from a marked redistribution of charge within the Ru t_{2g} shell, accompanied by a sudden collapse of the spectral weight in the lower Hubbard band and the emergence of a well defined Fermi surface which is devoid of pseudogaps. Our results highlight the profound roles of lattice energetics and of the multiorbital nature of Ca_2RuO_4 in this archetypal Mott transition and open new perspectives for spectroscopic measurements.

Main text:

Mott metal-insulator-transitions are driven by electron-electron interactions but often coincide with structural phase transitions [1]. While the latter were long believed to be a secondary response, as argued originally by N.F. Mott [2], realistic numerical studies point to a far more important role of structural changes in stabilizing the Mott state of archetypal insulators [3, 4]. This, together with recent theoretical advances, has led to renewed interest in the interplay of lattice energetics and electronic properties near Mott transitions [5–7]. Hydrostatic and uniaxial pressure is particularly important in the experimental study of Mott transitions and also has a profound effect on other emerging properties of quantum materials [1, 8–12]. However, conventional pressure cells are fundamentally incompatible with modern surface sensitive spectroscopies such as angle-resolved photoemission (ARPES). Consequently the evolution of the k -space electronic structure in Mott systems as they are tuned across the metal-insulator transition (MIT) has remained largely unknown. In order to overcome this limitation of ARPES, we developed an apparatus which is compatible with modern ARPES facilities and permits *in-situ* quasi-continuous tuning of uniaxial strain. Here, we use this new capability to investigate the layered perovskite Ca_2RuO_4 , which is of particular scientific interest as a prototypical multiband Mott insulator. Within band theory Ca_2RuO_4 is a good metal with a nearly uniform distribution of the 4 Ru d -electrons over the 3 t_{2g} orbitals. How such a multiband metal with fractional occupation can undergo

a Mott transition has been debated intensely, but the lack of data from the metallic state has prevented stringent tests of theoretical models [4, 13–17]. More recently the magnetic properties in the insulating state of Ca_2RuO_4 have attracted much interest [15, 18, 19] following proposals of a $J_{\text{eff}} = 0$ state with excitonic magnetism and an exotic doping evolution [20, 21] as well as the observation of unprecedented diamagnetism in a semimetallic phase induced by dc electric current [22].

The insulating state of Ca_2RuO_4 is known to be very sensitive to pressure [23–26], chemical substitution [27, 28] and even electric fields [22, 29]. To further increase the sensitivity of the insulating ground state of Ca_2RuO_4 to strain, we have grown a series of La, Nd and Pr doped single crystals. Details of the sample growth and characterization are given in the supplementary information. Despite the slightly different rare earth ionic radii these samples behave qualitatively similarly. We thus chose to concentrate on $\text{Ca}_{2-x}\text{Pr}_x\text{RuO}_4$ with $x = 0, 0.03, 0.04, 0.07$. Consistent with a previous study on La-doped Ca_2RuO_4 [28] we find that Pr does not introduce itinerant carriers in the insulating state but suppresses the structural phase transition accompanying the metal insulator transition (MIT) from $T_{MI} \sim 360$ K for $x = 0$ to ~ 85 K at the highest doping level of $x = 0.07$ used in our study (see phase diagram in Fig. 1a). Our single crystal neutron diffraction data show that the structural transition of $\text{Ca}_{2-x}\text{Pr}_x\text{RuO}_4$ is similar to the one in pure Ca_2RuO_4 . In particular, it is symmetry-preserving for all doping levels and mainly characterized by a flattening of the RuO_6 octahedra together with an elongation of the b -axis leading to strong orthorhombicity in the insulating phase [see supplementary information]. We will exploit this latter property to tune the MIT by uniaxial strain. Adopting the notation used for pure Ca_2RuO_4 , we call the metallic phase with long c -axis and $Pbca$ space group $L\text{-}Pbca$ and the insulating phase with short c axis $S\text{-}Pbca$.

Our *in-situ* transferable strain apparatus is shown in Fig. 1c. It is actuated mechanically by turning a screw, which causes a lever to press a stainless steel ball from below on a 1 mm thick CuBe substrate. The elastic deformation of the substrate results in tensile strain $\epsilon_{xx}^{\text{sub.}}$ along the bending direction on the upper surface and a much smaller compressive strain $\epsilon_{yy}^{\text{sub.}}$ in the orthogonal direction. We calibrate $\epsilon^{\text{sub.}}$ using finite element analysis, as shown in Fig. 1d and supplementary Fig. 2, taking into account the indent in the substrate left by the ball, which we measure at the end of each experiment. For a maximal coupling of in-plane strain to the c -axis compression, which putatively drives the MIT [4], we align the

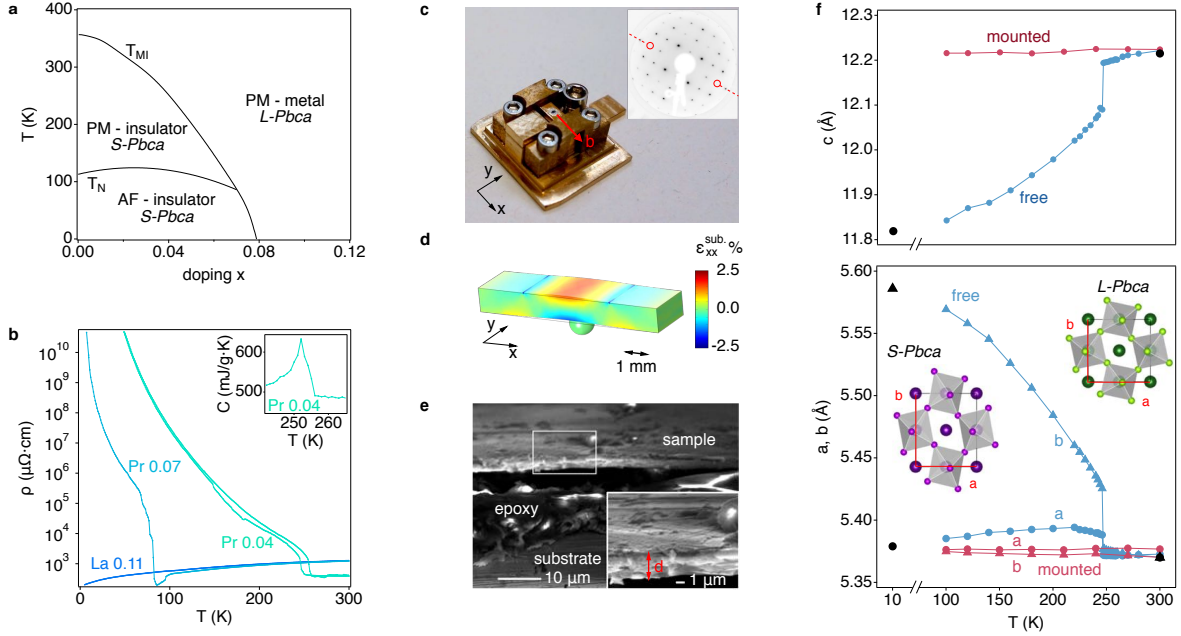


FIG. 1. **Phase diagram and strain apparatus.** **a** Metallic and insulating phases of $\text{Ca}_{2-x}\text{Pr}_x\text{RuO}_4$ are separated by a first order structural phase transition from $L\text{-Pbca}$ to $S\text{-Pbca}$. Canted antiferromagnetism is observed in all insulating samples below ≈ 110 K. **b** Resistivity curves for $\text{Ca}_{2-x}\text{Pr}_x\text{RuO}_4$ ($x = 0.04, 0.07$) and $\text{Ca}_{2-x}\text{La}_x\text{RuO}_4$ ($x = 0.11$), which we use as a reference for the metallic ground state. The hysteretic behavior shown for $x = 0.04$ confirms that the transition is first order. The inset shows the peak in the specific heat at the structural phase transition for $x = 0.04$. **c** Photograph of the strain apparatus. Bending the substrate along the b axis drives strained $\text{Ca}_{2-x}\text{Pr}_x\text{RuO}_4$ towards the insulating orthorhombic $S\text{-Pbca}$ ground state. The inset shows a LEED pattern of a strained sample, revealing the glide plane (dashed red line). **d** Calibration of the strain apparatus using finite element analysis. The color scale encodes the tensile strain. **e** Scanning electron micrograph of a cleaved and fully strained sample. The black region between sample and epoxy layer is due to a shadowing effect caused by the high roughness of the cut through sample and substrate. **f** Temperature dependence of the lattice constants for $x = 0.04$ measured by single crystal X-ray diffraction (XRD) before and after mounting the sample on our strain apparatus. We find that samples as thin as the one imaged in **e** preserve the high-temperature $L\text{-Pbca}$ structure down to base temperature. Black symbols indicate lattice constants obtained by single crystal neutron diffraction at 10 K and 300 K.

crystalline b -axis with the bending direction. Since this axis lies in a glide plane of the $Pbca$ structure, it can be identified readily in low-energy electron diffraction (LEED) patterns via the extinction of spots at certain energies (inset to Fig. 1c).

Key to our experiment is the exploitation of the initial compressive strain exerted by the large differential thermal contraction as apparatus and sample are cooled to base temperature. Using literature data for the CuBe substrates and our neutron diffraction data for $\text{Ca}_{2-x}\text{Pr}_x\text{RuO}_4$, we calculate nominal values of $\epsilon_{xx}^i = -4.1\%$ (-2.3%) for Pr concentrations $x = 0.04$ (0.07) [see supplementary information]. We directly confirm these exceptionally high strain levels for the most challenging case of a $x = 0.04$ sample using X-ray diffraction on cleaved samples mounted on our strain apparatus. From the data shown in Fig. 1f we calculate an initial compressive strain $\epsilon_{xx}^i = (b^{\text{mounted}} - b^{\text{free}})/b^{\text{free}} = -3.6\%$ at 100 K, in excellent agreement with the nominal value of -3.8% at this temperature. These strain levels are achieved by mounting ultrathin plate-like single crystals to minimize strain relaxation. Cross-sectional electron microscopy images of our mounted and cleaved samples indicate typical thicknesses of $\sim 10 \mu\text{m}$ for the epoxy layer and $2 - 10 \mu\text{m}$ for the single crystals (Fig. 1e). Having confirmed negligible relaxation at the highest strain used in our experiment, we approximate the total strain as $\epsilon^{\text{tot}} = \epsilon^i + \epsilon^{\text{sub}}$, where ϵ^i is compressive and ϵ^{sub} tensile.

From Fig. 1f it is evident that suitably mounted samples remain in the quasi-tetragonal L - $Pbca$ structure down to base temperature. Bending the substrate in our strain apparatus at low temperature then drives $\text{Ca}_{2-x}\text{Pr}_x\text{RuO}_4$ towards the orthorhombic S - $Pbca$ ground state. The striking effect of uniaxial strain on the electronic structure of $\text{Ca}_{2-x}\text{Pr}_x\text{RuO}_4$ is evident from the ARPES Fermi surfaces shown in Fig. 2a,b. For an unstrained sample in the S - $Pbca$ phase we find negligible intensity at the Fermi level E_F and no discernible structure in momentum space consistent with a gapped Mott insulating state. In a fully strained sample with L - $Pbca$ structure, on the other hand, a clear Fermi surface emerges, demonstrating a metallic ground state. Intriguingly, the strain-induced metallic state differs strongly from lightly doped cuprates and iridates [30, 31]. In particular, we find no anisotropy in the quasiparticle coherence and no evidence for a pseudogap along the entire Fermi surface within the precision of our experiment of $\approx 2 \text{ meV}$. A cut along the ΓY high-symmetry line (Fig. 2e, first panel) shows well defined, strongly renormalized quasiparticle states at very low energy only indicating a delicate Fermi liquid regime. Beyond a coherence scale of $\sim 30 \text{ meV}$,

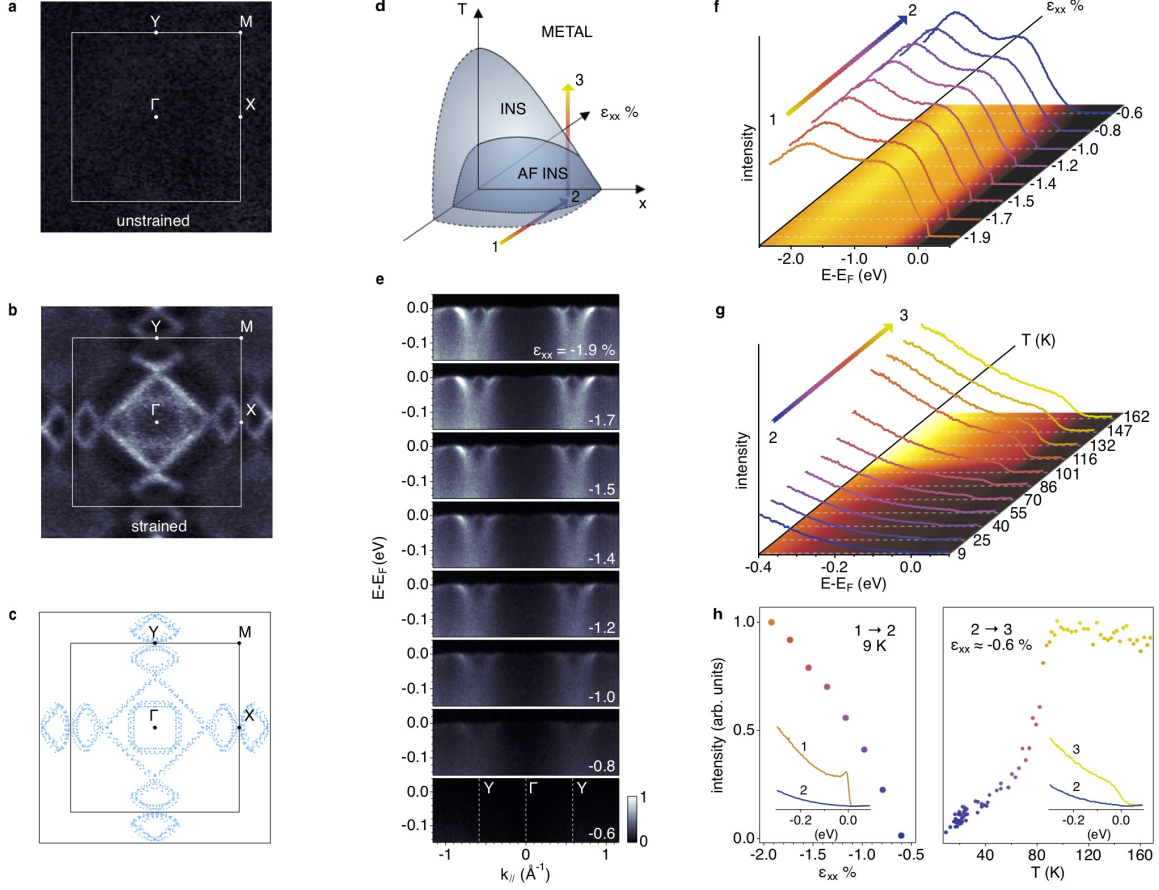


FIG. 2. **Strain tuning of the MIT and nature of the low-temperature metallic state.** **a,b** ARPES Fermi surface maps for a $x = 0.07$ sample and a fully strained $x = 0.04$ sample measured at 50 K and 8 K, respectively. The former was measured on a sufficiently thick sample to cause almost complete relaxation of the initial strain. The data were acquired using 64 eV photons with linear horizontal polarization. **c** Fermi surface contours extracted from the data in **b**. **d** Schematic three dimensional *strain-doping-temperature* phase diagram of $\text{Ca}_{2-x}\text{Pr}_x\text{RuO}_4$. **e** Evolution of the quasiparticle band structure at 8 K along YTY as the strain is tuned along the path 1 \rightarrow 2 in **a**. **f** Angle-integrated energy distribution curves (EDCs) over the full width of the occupied Ru t_{2g} states as a function of uniaxial strain. **g** Angle-integrated EDCs as a function of temperature measured at minimum strain $\epsilon_{xx}^i \approx -0.6\%$ (path 2 \rightarrow 3). The sample undergoes the MIT at ~ 90 K. **h** Evolution of the spectral weight at the Fermi level along the path 1 \rightarrow 2 \rightarrow 3 defined in **d**.

the excitations broaden rapidly and their dispersion increases simultaneously. These high-

energy states can be tracked down to ~ -2.7 eV and thus essentially over the full bare band width (see Fig. 3). Such a coexistence of heavy quasiparticles with 'unrenormalized' high-energy states was identified as a hallmark of Hund's metals with profound implications on magnetic susceptibility, thermal and electrical transport [32].

Subsequently, we use our strain apparatus to tune across the Mott transition. Fig. 2e,f shows the evolution of the near- E_F electronic structure for a $x = 0.07$ sample following the path 1 \rightarrow 2 in the schematic phase diagram of Fig. 2d. Clearly, we achieve a sufficient tuning range to fully recover the characteristic spectrum of insulating $\text{Ca}_{2-x}\text{Pr}_x\text{RuO}_4$ with an exponential onset of weight. The angle-resolved data show that the Mott transition is approached by a uniform reduction of the spectral weight. Interestingly though, the quasiparticle dispersion is not affected strongly by strain. We can thus exclude that the strain-induced Mott transition is triggered by a divergence of the effective mass predicted in the Brinkmann-Rice model [33]. Raising the temperature (2 \rightarrow 3, Fig. 2g), the insulating state undergoes another phase transition close to T_{MI} of the unstrained state and we recover a metallic spectrum with significant weight at E_F . As shown in Fig. 2e,f, the suppression of the spectral weight at E_F during the strain-tuning is gradual. This can either indicate a second order phase transition or a phase coexistence with domains below the lateral dimension of $\approx 20 \times 50 \mu\text{m}$ probed by ARPES. Given the sensitivity of the electronic state of $\text{Ca}_{2-x}\text{Pr}_x\text{RuO}_4$ to its first order structural phase transition, we consider the latter more likely. Additional evidence for phase coexistence, which was also observed in diffraction experiments on Ca_2RuO_4 under hydrostatic pressure [24], is shown in supplementary information.

The Fermi surface of strained $\text{Ca}_{2-x}\text{Pr}_x\text{RuO}_4$ is remarkably simple considering the large unit cell containing 4 formula units and 16 electrons in the Ru t_{2g} shell. We find a square hole-like sheet centered at Γ , which encloses a smaller electron-like Fermi surface, and four small lens-shaped sheets at the X and Y points, respectively. The absence of exchange splitting in our experimental data indicates a paramagnetic metallic state, as it is also observed in the $L\text{-Pbca}$ phase of undoped Ca_2RuO_4 and for highly La-doped Ca_2RuO_4 with $L\text{-Pbca}$ structure in the ground state [28]. We thus conclude that the low-temperature metallic state induced by uniaxial strain in our experiments represents the intrinsic metallic phase of Ca_2RuO_4 but differs from bulk crystals under hydrostatic pressure and from epitaxially strained thin films, where ferromagnetism with an ordered moment of $0.1 \div 0.3 \mu_B$ is observed below ~ 20 K [23, 25, 26].

Measuring the Fermi surface volume, we find approximate electron-hole compensation, consistent with a localized character of the Pr excess electrons. Doping dependent measurements (not shown), on the other hand indicate a measurable change of the Fermi surface volume with doping x , suggesting an at least partial delocalization of the dopants in the metallic $L-Pbca$ phase. Due to the large rotation of the RuO_6 octahedra and the sizeable spin-orbit coupling, we cannot uniquely identify the orbital character on the Fermi surface from linear dichroism measurements. However, it appears plausible to interpret the extended straight sections of the experimental Fermi surface as originating predominantly from the quasi-1d xz, yz orbitals while the curved sections of the lens-pockets as well as the circular pocket at Γ are likely of dominant xy character. Based on this interpretation, we estimate the orbital polarization in the metallic state using a simple tight-binding model fitted to the experimental Fermi surface contours. This suggest orbital occupations $n_{xz} \approx n_{yz} \approx 1.4$ and $n_{xy} \approx 1.2$, and thus a strongly reduced polarization $p = n_{xy} - (n_{xz} + n_{yz})/2 \approx 0 \div 0.4$ with respect to the insulating state characterized in previous work [4, 7, 16, 17].

Further evidence of a large redistribution of spectral weight at the strain-induced MIT comes from the ARPES data over a larger energy scale. In Fig. 3a,c we compare dispersion plots covering the full width of the t_{2g} shell from two insulating and paramagnetic samples with $S-Pbca$ structure and $x = 0, 0.03$ with a fully strained sample of comparable doping $x = 0.04$ in the $L-Pbca$ structure.

The first important conclusion from this data is that light Pr-doping alone causes minor changes in the electronic structure only. Its main effect is a small shift of the chemical potential. Importantly though, E_F remains in the correlated gap, consistent with the highly insulating nature of $x = 0.03$ crystals in resistivity measurements. We therefore conclude that the additional valence electron of Pr stays fully localized in the insulating $S-Pbca$ structure, possibly due to a Mott transition in the impurity band, as it was proposed for lightly La-doped Sr_2IrO_4 [34]. The main spectroscopic features in the insulating phase are a dispersive state with ≈ 2 eV bandwidth and an intense non-dispersive peak at -1.7 eV. With reference to our dynamical mean field theory (DMFT) calculations (Fig. 3d) and consistent with Ref. [17], we identify these features with the fully occupied xy orbital and the lower Hubbard band (LHB) of xz/yz character, respectively. This confirms a basic electronic configuration in the insulating $S-Pbca$ phase with fully occupied d_{xy} orbital and half-filled d_{xz}/d_{yz} bands split into lower and upper Hubbard band, as proposed on the basis of DMFT

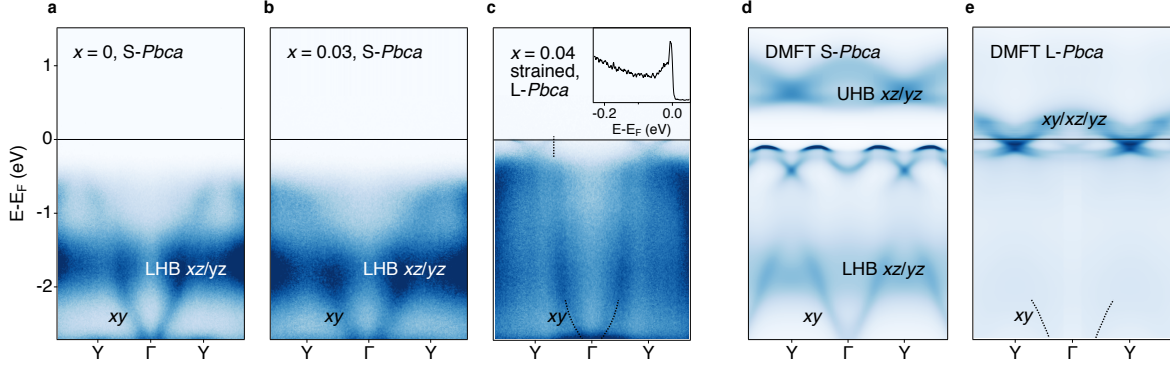


FIG. 3. **Redistribution of spectral weight across the MIT.** ARPES spectral weight along ΓY measured for different dopings and structures: **a** undoped Ca_2RuO_4 at 180 K ($S\text{-}Pbca$, paramagnetic); **b** $x = 0.03$ at 150 K ($S\text{-}Pbca$, paramagnetic); **c** fully strained $x = 0.04$ at 10 K ($L\text{-}Pbca$, metallic). We display a superposition of data acquired with left and right circular polarization; the inset in **c** shows a clear quasi-particle peak at $k=k_F$ (dotted line); **d,e** DMFT calculation along the same cut for undoped Ca_2RuO_4 in the $S\text{-}Pbca$ and $L\text{-}Pbca$ structure at $T=232$ K and 390 K, respectively. The bottom of the xy band, which becomes visible upon enhancing the contrast in the DMFT calculation of the metallic state is indicated by a dotted line in **c,e**.

calculations [4, 14].

Straining a lightly doped $\text{Ca}_{2-x}\text{Pr}_x\text{RuO}_4$ sample, we observe a substantial redistribution of spectral weight. Most notably, the intensity in the LHB collapses suddenly across the MIT and coherent quasiparticle states appear at the chemical potential (Fig. 3c). Both of these effects are reproduced by our DMFT calculations shown in Fig. 3e. Interestingly though, the sudden collapse of the LHB is in stark contrast to lightly doped cuprates, where metallicity emerges from a gradual transfer of spectral weight from the LHB to coherent quasiparticle states [35]. We interpret this as a generic manifestation of the additional orbital degree of freedom of multiband Mott insulators. In effective single band systems, such as the cuprates or iridates, the orbital occupancy can only change by the small number of doped carriers, resulting in dominantly half-filled sites retaining a strong memory of the Mott phase. In $\text{Ca}_{2-x}\text{Pr}_x\text{RuO}_4$, on the other hand, our data show a discontinuous change of the $n_{xz/yz}$ occupancy from 1 to ≈ 1.4 in spite of the only light doping because of substantial interorbital charge transfer across the MIT. The large deviation from half filling causes a sudden collapse of the LHB and renders electronic energies comparable to lattice energies

under strain, resulting in a strongly first order nature of the Mott transition.

Our results show that tuning uniaxial strain in ARPES experiments is a promising new method to study phase transitions or, more generally, structure – property relations of quantum materials. Potential applications of our method range from tuning magnetism, to topological phase transitions, two-dimensional van der Waals materials and unconventional superconductors showing large responses to strain, such as Sr_2RuO_4 [11].

Methods:

Single crystals of $\text{Ca}_{2-x}\text{Pr}_x\text{RuO}_4$ were grown through the floating zone (FZ) technique using a Crystal System Corporation FZ-T-10000-H-VI-VPO-I-HR-PC four mirror optical furnace. Samples were grown in 90% oxygen pressure, and the initial Ru concentration in the polycrystalline rods was about 20% higher than the nominal value to compensate for evaporation during the growth. The bulk properties were thoroughly characterized by resistivity, specific heat, magnetization measurements, and single crystal neutron diffraction at the ISIS spallation neutron source [36]. Doping levels were measured by energy and wavelength dispersive X-ray spectroscopy (EDX/WDX) and were found to be systematically lower by 20% to 30% than in the polycrystalline growth rod. Angle-resolved photoemission spectroscopy (ARPES) experiments were performed at the I05 Beamline of the Diamond Light Source [37]. The presented data were acquired with linearly and circularly polarized light at 64 eV photon energy and an overall resolution of $\approx 12 \text{ meV} / 0.015 \text{ \AA}^{-1}$.

We thank E. Giannini, D. McMorro, D. Pincini, D. Jaccard, C. Renner, M. Spera, V. Pasquier for discussions, J. Teyssier for Raman experiments on $\text{Ca}_{2-x}\text{Pr}_x\text{RuO}_4$, M. Spera for help with the numerical strain simulations and R. Pellet for machining and aligning the strain apparatus. The experimental work was supported by the Swiss National Science Foundation (200021-153405 and 200020-165791). Theoretical work was supported by the European Research Council grant ERC-319286-QMAC, the NCCR MARVEL of the SNSF and the Simons Foundation (Flatiron Institute). Crystal growth and characterization at UCL was supported by the EPSRC grant EP/N034694/1. We gratefully acknowledge the Science and Technology Facilities Council (STFC) for access to neutron beamtime at ISIS, and also for the support of sample preparation at the UCL crystal growth laboratory. We

would like to thank G. Stenning for help on the Smartlab XRD and Quantum Design MPMS instruments in the Materials Characterisation Laboratory at the ISIS Neutron and Muon Source. We acknowledge Diamond Light Source for time on beamline I05 under proposal SI17381.

* New permanent address: Deutsches Elektronen-Synchrotron DESY, Photon Science, Hamburg, 22607, Germany

- [1] Imada, M., Fujimori, A. & Tokura, Y. Metal-insulator transitions. *Rev. Mod. Phys.* **70**, 1039 (1998). URL <http://link.aps.org/abstract/RMP/v70/p1039>.
- [2] Mott, N. F. The basis of the electron theory of metals, with special reference to the transition metals. *Proceedings of the Physical Society. Section A* **62**, 416 (1949). URL <http://stacks.iop.org/0370-1298/62/i=7/a=303>.
- [3] Pavarini, E. *et al.* Mott transition and suppression of orbital fluctuations in orthorhombic 3d¹ perovskites. *Phys. Rev. Lett.* **92**, 176403 (2004). URL <http://link.aps.org/doi/10.1103/PhysRevLett.92.176403>.
- [4] Gorelov, E. *et al.* Nature of the Mott transition in Ca₂RuO₄. *Phys. Rev. Lett.* **104**, 226401 (2010). URL <https://link.aps.org/doi/10.1103/PhysRevLett.104.226401>.
- [5] Park, H., Millis, A. J. & Marianetti, C. A. Total energy calculations using DFT+ DMFT: Computing the pressure phase diagram of the rare earth nickelates. *Phys. Rev. B* **89**, 245133 (2014). URL <https://link.aps.org/doi/10.1103/PhysRevB.89.245133>.
- [6] Leonov, I., Anisimov, V. I. & Vollhardt, D. First-principles calculation of atomic forces and structural distortions in strongly correlated materials. *Phys. Rev. Lett.* **112**, 146401 (2014). URL <https://link.aps.org/doi/10.1103/PhysRevLett.112.146401>.
- [7] Han, Q. & Millis, A. Lattice energetics and correlation-driven metal-insulator transitions: the case of Ca₂RuO₄. *arXiv:1801.06215* 1–10 (2018). URL <http://arxiv.org/abs/1801.06215>.
- [8] Mathur, N. D. *et al.* Magnetically mediated superconductivity in heavy fermion compounds. *Nature* **394**, 39 (1998). URL <http://dx.doi.org/10.1038/27838>.
- [9] Schlom, D. G. *et al.* Strain tuning of ferroelectric thin films. *Annual Review of Materials Research* **37**, 589–626 (2007). URL <https://doi.org/10.1146/annurev.matsci.37.061206.113016>.

- [10] Drozdov, A. P., Erements, M. I., Troyan, I. A., Ksenofontov, V. & Shylin, S. I. Conventional superconductivity at 203 kelvin at high pressures in the sulfur hydride system. *Nature* **525**, 73 (2015). URL <http://dx.doi.org/10.1038/nature14964>.
- [11] Hicks, C. W. *et al.* Strong increase of T_c of Sr_2RuO_4 under both tensile and compressive strain. *Science* **344**, 283–285 (2014). URL <http://science.sciencemag.org/content/344/6181/283>.
- [12] Burganov, B. *et al.* Strain control of fermiology and many-body interactions in two-dimensional ruthenates. *Phys. Rev. Lett.* **116**, 197003 (2016). URL <https://link.aps.org/doi/10.1103/PhysRevLett.116.197003>.
- [13] Anisimov, V. I., Nekrasov, I. A., Kondakov, D. E., Rice, T. M. & Sigrist, M. Orbital-selective Mott-insulator transition in $\text{Ca}_{2-x}\text{Sr}_x\text{RuO}_4$. *Eur. Phys. J. B* **25**, 191–201 (2002). URL <https://doi.org/10.1140/epjb/e20020021>.
- [14] Liebsch, A. & Ishida, H. Subband Filling and Mott Transition in $\text{Ca}_{2-x}\text{Sr}_x\text{RuO}_4$. *Phys. Rev. Lett.* **98**, 216403–216404 (2007). URL <https://doi.org/10.1103/PhysRevLett.98.216403>.
- [15] Zhang, G. & Pavarini, E. Mott transition, spin-orbit effects, and magnetism in Ca_2RuO_4 . *Phys. Rev. B* **95**, 075145 (2017). URL <https://link.aps.org/doi/10.1103/PhysRevB.95.075145>.
- [16] Kubota, M. *et al.* Ferro-type orbital state in the Mott transition system $\text{Ca}_{2-x}\text{Sr}_x\text{RuO}_4$ studied by the resonant X-ray scattering interference technique. *Phys. Rev. Lett.* **95**, 026401 (2005). URL <https://link.aps.org/doi/10.1103/PhysRevLett.95.026401>.
- [17] Sutter, D. *et al.* Hallmarks of Hund's coupling in the Mott insulator Ca_2RuO_4 . *Nature Communications* **8**, 15176 (2017). URL <http://dx.doi.org/10.1038/ncomms15176>.
- [18] Kunkemöller, S. *et al.* Highly anisotropic magnon dispersion in Ca_2RuO_4 : evidence for strong spin orbit coupling. *Phys. Rev. Lett.* **115**, 247201 (2015). URL <https://link.aps.org/doi/10.1103/PhysRevLett.115.247201>.
- [19] Jain, A. *et al.* Higgs mode and its decay in a two-dimensional antiferromagnet. *Nature Physics* **13**, 633 EP – (2017). URL <http://dx.doi.org/10.1038/nphys4077>.
- [20] Khaliullin, G. Excitonic magnetism in Van Vleck-type d^4 Mott insulators. *Phys. Rev. Lett.* **111**, 197201 (2013). URL <https://link.aps.org/doi/10.1103/PhysRevLett.111.197201>.
- [21] Chaloupka, J. & Khaliullin, G. Doping-induced ferromagnetism and possible triplet pairing in d^4 mott insulators. *Phys. Rev. Lett.* **116**, 017203 (2016). URL <https://link.aps.org/>

- doi/10.1103/PhysRevLett.116.017203.
- [22] Sow, C. *et al.* Current-induced strong diamagnetism in the Mott insulator Ca_2RuO_4 . *Science* **358**, 1084–1087 (2017). URL <http://science.sciencemag.org/content/358/6366/1084>.
- [23] Nakamura, F. *et al.* From Mott insulator to ferromagnetic metal: a pressure study of Ca_2RuO_4 . *Phys. Rev. B* **65**, 220402 (2002). URL <https://link.aps.org/doi/10.1103/PhysRevB.65.220402>.
- [24] Steffens, P. *et al.* High-pressure diffraction studies on Ca_2RuO_4 . *Phys. Rev. B* **72**, 094104 (2005). URL <https://link.aps.org/doi/10.1103/PhysRevB.72.094104>.
- [25] Miao, L. *et al.* Itinerant ferromagnetism and geometrically suppressed metal-insulator transition in epitaxial thin films of Ca_2RuO_4 . *Applied Physics Letters* **100**, 052401 (2012). URL <https://doi.org/10.1063/1.3680250>.
- [26] Dietl, C. *et al.* Tailoring the electronic properties of Ca_2RuO_4 via epitaxial strain. *Applied Physics Letters* **112**, 031902 (2018). URL <https://doi.org/10.1063/1.5007680>.
- [27] Nakatsuji, S. & Maeno, Y. Quasi-two-dimensional Mott transition system $\text{Ca}_{2-x}\text{Sr}_x\text{RuO}_4$. *Phys. Rev. Lett.* **84**, 2666 (2000). URL <https://doi.org/10.1103/PhysRevLett.84.2666>.
- [28] Fukazawa, H. & Maeno, Y. Filling Control of the Mott Insulator Ca_2RuO_4 . *Journal of the Physical Society of Japan* **70**, 460–467 (2001). URL <https://doi.org/10.1143/JPSJ.70.460>.
- [29] Nakamura, F. *et al.* Electric-field-induced metal maintained by current of the Mott insulator Ca_2RuO_4 . *Scientific Reports* **3**, 2536 (2013). URL <http://dx.doi.org/10.1038/srep02536>.
- [30] Damascelli, A. Angle-resolved photoemission studies of the cuprate superconductors. *Review of Modern Physics* **75**, 473 (2003).
- [31] De La Torre, A. *et al.* Collapse of the Mott Gap and Emergence of a Nodal Liquid in Lightly Doped Sr_2IrO_4 . *Physical Review Letters* **115**, 2–6 (2015).
- [32] Georges, A., de’ Medici, L. & Mravlje, J. Strong electronic correlations from Hund’s coupling (2012). URL <http://arxiv.org/abs/1207.3033> <http://dx.doi.org/10.1146/annurev-conmatphys-020911-125045>.
- [33] Brinkman, W. F. & Rice, T. M. Application of gutzwiller’s variational method to the metal-insulator transition. *Phys. Rev. B* **2**, 4302–4304 (1970). URL <https://link.aps.org/doi/10.1103/PhysRevB.2.4302>.
- [34] Battisti, I. *et al.* Universality of pseudogap and emergent order in lightly doped mott insula-

- tors. *Nature Physics* **13**, 21 (2016). URL <http://dx.doi.org/10.1038/nphys3894>.
- [35] Shen, K. M. *et al.* Missing quasiparticles and the chemical potential puzzle in the doping evolution of the cuprate superconductors. *Phys. Rev. Lett.* **93**, 267002 (2004). URL <https://doi.org/10.1103/PhysRevLett.93.267002>.
- [36] Keen, D. A., Gutmann, M. J. & Wilson, C. C. SXD – the single-crystal diffractometer at the ISIS spallation neutron source. *Journal of Applied Crystallography* **39**, 714–722 (2006). URL <https://doi.org/10.1107/S0021889806025921>.
- [37] Hoesch, M. *et al.* A facility for the analysis of the electronic structures of solids and their surfaces by synchrotron radiation photoelectron spectroscopy. *Review of Scientific Instruments* **88**, 013106 (2017). URL <https://doi.org/10.1063/1.4973562>.